Chemical Engineering Journal 313 (2017) 317–327

Contents lists available at ScienceDirect

Chemical Engineering Journal

journal homepage: www.elsevier.com/locate/cej

Supercritical fluid coating of API on excipient enhances drug release

Qingguo Li [a], Deen Huang [a], Tiejun Lu [b], Jonathan P.K. Seville [c], Lei Xing [b], Gary A. Leeke [d,*]

[a] School of Chinese Materia Medica, Guangzhou University of Chinese Medicine, Guangzhou 510006, PR China
[b] Centre for Formulation Engineering, School of Chemical Engineering, University of Birmingham, B15 2TT, UK
[c] Department of Chemical and Process Engineering, University of Surrey, Guildford, Surrey GU2 7XH, UK
[d] School of Water, Energy and Environment, Cranfield University, Cranfield, Bedfordshire MK43 0AL, UK

HIGHLIGHTS

- Supercritical Anti-Solvent process is combined with pressurised fluidised bed.
- Nanoparticles of organic active are captured.
- Spherical morphology of naringin active coated on excipient surface.
- High coating loadings of active obtained.
- Release of active from excipient is enhanced compared to conventional fluidised bed.

GRAPHICAL ABSTRACT

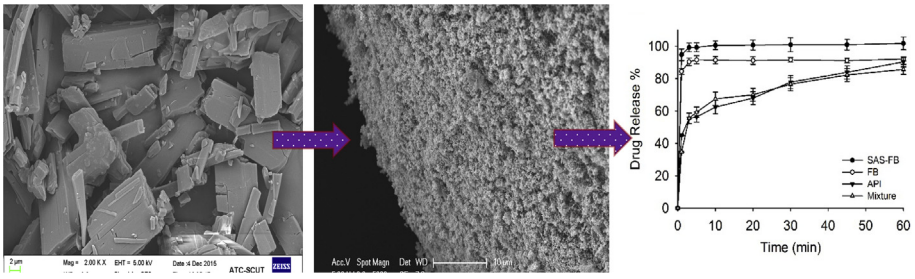

ARTICLE INFO

Article history:
Received 27 July 2016
Received in revised form 2 December 2016
Accepted 14 December 2016
Available online 18 December 2016

Chemical compounds studied in this article:
Carbon dioxide (PubChem CID: 280)
Naringin (PubChem CID: 442428)

Keywords:
Supercritical Anti-Solvent
Fluidized bed coating
Naringin
Release profile
Nanoparticles

ABSTRACT

A process to coat particles of active pharmaceutical ingredient (API) onto microcrystalline cellulose (MCC) excipient shows promise as a new way to dosage forms showing enhanced drug release. The process consists of a fluidized bed operated at elevated pressure in which API particles are precipitated from a Supercritical Anti-Solvent process (SAS). MCC particles were used as an excipient in the fluidized bed and collect the SAS-generated API particles. Naringin was selected as the model API to coat onto MCC. A number of operational parameters of the process were investigated: fluidization velocity, coating pressure, temperature, concentration of drug solution, drug solution flow rate, drug mass, organic solvent, MCC mass and size and CO_2-to-organic solution ratio. SEM and SPM analyses showed that the MCC particle surfaces were covered with near-spherical nanoparticles with a diameter of approximately 100–200 nm, substantially smaller than the as-received API material. XRD showed that naringin changed from crystalline to amorphous during processing. The coated particles resulting from the SAS fluidized bed process have a higher loading of API, gave faster release rates and higher release ratios in comparison with those produced using a conventional fluidized bed coating process. The approach could be transferred to other industries where release is important such as agrochemical, cosmetic and food.

1. Introduction

Active pharmaceutical ingredients (API) in nanoparticulate form have advantageous properties, such as higher dissolute rate and greater bioavailability than those prepared by conventional approaches [1]. This is attributed to an enhanced dissolution rate due to the particle size and intrinsic solubility. Previous studies on a number of poorly soluble drugs have demonstrated that particle size reduction resulted in an increase rate of dissolution and higher oral bioavailability [2].

Nanosizing in the pharmaceutical industry refers to the reduction of the API particle size down to a sub-micron range [3]. Over the past few decades, a range of processes including milling,

* Corresponding author.
E-mail address: takeuchi@ee.e.titech.ac.jp (G.A. Leeke).

http://dx.doi.org/10.1016/j.cej.2016.12.066
1385-8947/

precipitation and homogenization have been employed by the pharmaceutical industry to reduce the particle size, in order to achieve desired performance. However, nanoparticles are not readily attainable through conventional routes and a subsequent comminuting stage is often necessary, which involves large amounts of energy input and may alter the physicochemical properties of the product [1,4].

To address the above mentioned technical challenges in generating sub-micron particles, it has been demonstrated that the micronization using supercritical fluids routes [5,6], especially the Supercritical Anti-Solvent (SAS) process, has great potential [7–11]. The SAS process makes use of the high solvent power of supercritical fluids to dissolve certain organic solvents and to act as an anti-solvent to drugs that have no or low solubility in the selected supercritical fluid, thereby causing their simultaneous precipitation. In a typical SAS process, the API of choice is dissolved in an organic solvent and is injected into the supercritical fluid through a small diameter nozzle, which rapidly causes its supersaturation and precipitation as a result of the instantaneous miscibility of the supercritical fluid with the organic solvent. Due to the high and uniform degree of supersaturation, small particles of API with a narrow particle size distribution are obtained. The SAS process has been proven to be effective in preparing nanoparticles for many active drugs [11].

Several authors have combined supercritical fluids and fluidized beds in the past to coat materials in a fluidized bed. Some researchers have reported a fluidized bed process operating at ambient pressure to capture particles (not APIs) or wax from a supercritical CO_2 stream flowing into the bed [12,13], in a process similar to RESS (Rapid Expansion of Supercritical Solutions). Others have described the fluid dynamics of a fluidized bed operating at supercritical conditions [14] and have subsequently operated the fluidized bed [15] and injected CO_2 laden with wax to coat glass beads. Rosenkranz et al. [16] have used a variation of the process to precipitate a protein from aqueous solution onto a supercritical CO_2 fluidized bed of lactose, while simultaneously injecting a supercritical mixture of CO_2 and paraffin at high temperature and pressure which encapsulates the BSA protein on the lactose. A recent paper [17] describes a process to coat polymer film from an ethanol solution onto titanium particles by precipitation from a supercritical carbon dioxide fluidized bed. However, until the current work there has been no experimental demonstration of the use of SAS within a pressurized fluidized bed to coat API particles, with proof of their release properties. The process captures the SAS generated nanoparticles onto excipient carrier particles causing build-up of a coating. The immediate collection of nanoparticles in the process onto an excipient close to their point of origin, prevents further particle growth and agglomeration, forming a product which retains the efficacy and special features of the nanometer size in an easily handleable form. The process combination could potentially offer an even greater opportunity to significantly improve the coating properties, whilst retaining and taking advantage of the nanoparticulate form of the API in drug release applications. The approach could be transferred to other industries where release is important such as agrochemical, cosmetic and food.

Naringin ($C_{27}H_{32}O_{14}$, CAS: 10236-47-2) is a double hydrogen flavonoid compound and has antioxidant, anti-inflammatory, anticancer, anti-allergic and anti-diabetic properties. The solubility of naringin in water (20 °C) is poor, which leads to low bioavailability and hinders further studies on its pharmacological actions [18–20].

The work reported here uses naringin as a model drug in a Supercritical Anti-Solvent Fluidized Bed process in order to improve its dissolution properties. A number of parameters were studied in order to optimize the process: the fluidization velocity, coating pressure, temperature, concentration of drug solution, drug solution flow rate, drug mass, organic solvent, MCC mass and size and CO_2-to-organic solution ratio. The drug release profiles of the coated composite particles were determined.

2. Experimental

2.1. Materials

All materials were used as purchased without further purification: Naringin (99.0%) was donated by Professor Su Weiwei (Sun Yat-sun University, PR China); Carbon dioxide ($\geqslant$99.8%) was purchased from BOC UK; Microcrystalline cellulose: Ethispheres 150, 250 and 450, with particle size ranges of: 100–200, 200–355 and 355–500 μm, respectively, and particle density of 1.4 g/cm^3 were imported from NP Pharm, Bazainville, France. Methanol $\geqslant$ 99.8%, ethanol $\geqslant$ 99.8% and acetone $\geqslant$ 99.8% were all bought from Sigma-Aldrich Company Ltd. Dorset, UK.

2.2. Apparatus

The experiments were carried out in a SAS-fluidized bed (SASFB) coating rig developed in-house. Fig. 1 shows a schematic of the SAS fluidized bed coating equipment in which a former SAS rig [7] was modified to accommodate a fluidized bed located inside a high pressure vessel (HPV). Supercritical CO_2 was introduced from the bottom of the HPV which acted as an anti-solvent, causing precipitation of the naringin from the selected organic solvent solution. The CO_2 also acted as fluidizing gas for the MCC excipient particles within the vessel. The organic solvent or organic solution containing naringin was injected by a HPLC pump at the desired flow rate into the MCC fluidized bed where the precipitating API particles produced by the SAS process were coated onto the MCC. A 90 μm sintered plate gas distributor is located at the base of the fluidized bed to ensure a uniform sc-CO_2 flow; a 127 μm ID stainless steel capillary is used as the nozzle, through which the organic solution was injected into the CO_2 stream and MCC bed.

The MCC was held in a conical glass tube fitted on the top of brass plenum chamber (see Figs. 1 and 2) to form a fluidized bed through which the sc-CO_2/organic solvent (solution) passes; and the coating process occurs. The diameter of the fluidized bed at the base was 6.5 mm giving a cross sectional area of 33.18 mm^2. Due to the conical nature of the tube, the cross-sectional area of the bed surface increased with the mass of MCC loaded. In the tests typically 1 to 4 g MCC was used; for a bed mass of 1 g the associated bed diameter was 12.6 mm, for 2 g this was 14.2 mm and for 4 g it was 18.4 mm.

A mesh filter with 44 μm openings was fitted on the top of the glass tube to prevent MCC being blown out from the bed. The sc-CO_2/organic solvent phase was depressurized to *c.* 20 bar and entered a middle pressure vessel (MPV), where the solvent was separated and recovered. Solvent-free CO_2 then passed through a cyclone to remove any residual solid and liquid prior to venting.

2.3. SAS-fluidized bed coating procedure

MCC particles were charged into the glass tube of the fluidized bed before the high pressure vessel was closed. Supercritical CO_2 was introduced into the vessel from the top of the HPV (not shown in Fig. 1) until the desired pressure was reached. Once the pressure stabilized the CO_2 inlet was switched from the top to the bottom of the HPV, allowing it to pass through the MCC to create the fluidized bed. Naringin was dissolved in organic solvent at the desired concentration. When the pressure, temperature and fluidized bed were stable, the pure organic solvent was injected into the

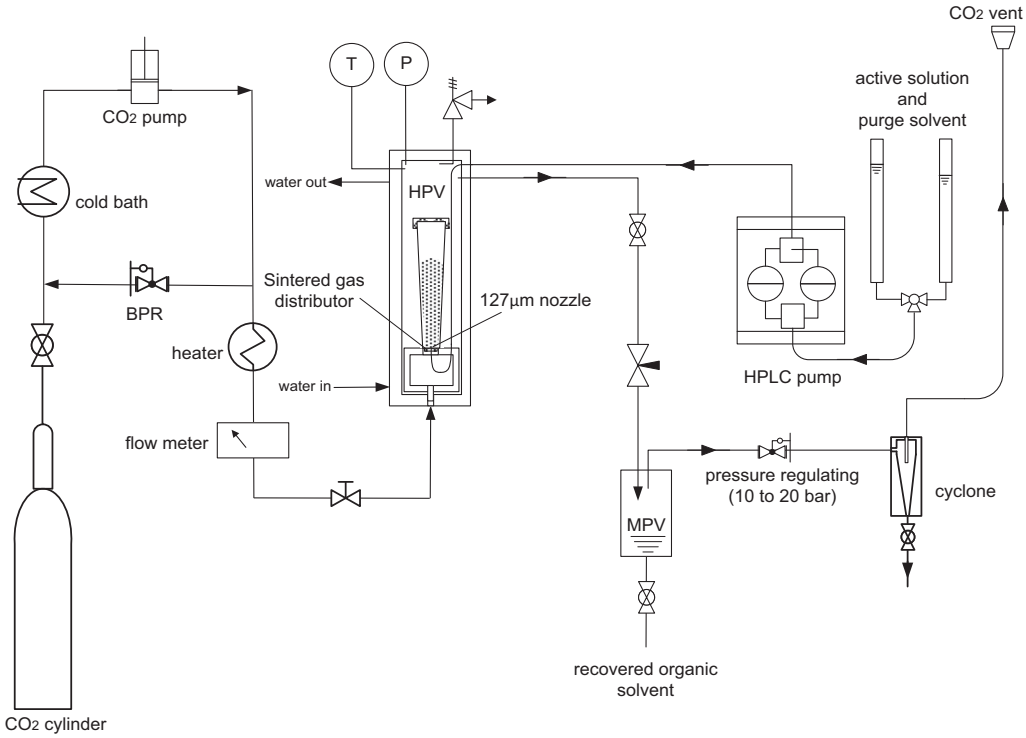

Fig. 1. Schematic of the SAS-fluidized bed rig. Flow meter = Rheonik Rhe08, HPV = Baskerville, UK pressure vessel max working P 300 bar at 100 °C; BPR = Tescom 26-1762-24, Germany; HPLC = Waters M-6000, Waters Associates, USA.

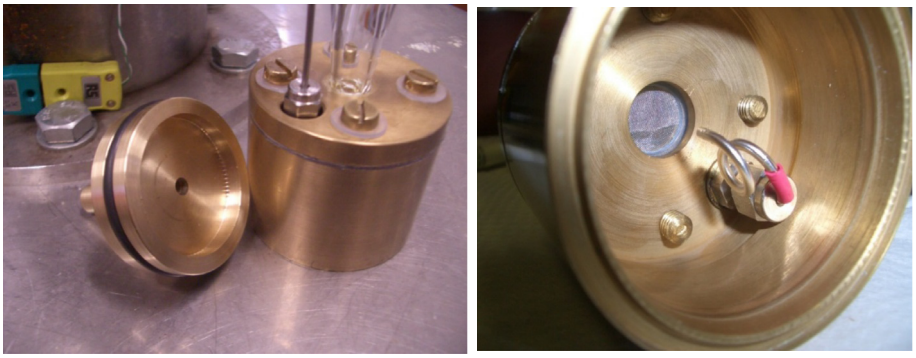

Fig. 2. Image of the plenum with the base of the glass fluidized bed attached, left; and underside of plenum showing nozzle tube to inject organic solution of API, right.

fluidized bed to purge and equalize the system pressure. The solvent was then switched to the naringin solution to start the coating process. After the desired coating time had passed, the solution flow was reverted to the pure solvent to purge the pipe lines at the same flow rate as the process while maintaining a constant CO_2 flow. After 10 mL purge solvent passed, the organic solvent pump was stopped and CO_2 was purged for a further 30 min to wash the fluidized MCC particles, so removing any residual solvent. The pressure was then reduced to atmospheric in stages. Once at ambient, the Naringin-coated MCC particles were removed from the fluidized bed for further characterization.

2.4. Optimization of SAS fluidized bed process

The fluidizing velocity, coating pressure, temperature, concentration of drug solution, drug solution flow rate, drug mass, organic solvent, MCC mass, CO_2-to-organic solution ratio, and the MCC diameter are considered the most important parameters for investigation in the SASFB process. The optimization of the operating conditions for the coating process was carried out systematically.

The procedure consisted of manipulating the nine variables which are listed in Tables 1 and 2. The drug release ratio and the loading of naringin on MCC were chosen as response variables to compare the coating results. The nine variables and their ranges (shown in parentheses) used in the experiments were coating pressure (80, 120, 150 bar), coating temperature (35, 40, 50 °C), naringin solution concentration (2.5, 5.0, 10.0, 15.0 mg/mL), drug solution flow rate (0.3, 0.5, 1.0, 1.5 mL/min), MCC mass (1.0, 2.0, 4.0 g, MCC particle average diameter (175, 295, 444 μm), (measured by Helos (H2290) & Rodos, Sympatec GmbH, Clausthal-Zellerfeld, Germany), total drug mass used per test (25.0, 50.0, 75.0, 100.0 mg), carbon dioxide flow rate (12, 25, 40 g/min), and solvent choice (ethanol, methanol, acetone). The ranges of each variable were based on the results of preliminary experiments.

2.5. Conventional fluidized bed coating procedure

A conventional fluidized bed coating process (test 23) was used to benchmark the SAS-fluidized bed performance. Twenty grammes of MCC particles were coated with naringin using a

Table 1
The nine variables and ranges used in the experimental study.

P bar	T °C	$F_{drug\ solution}$ mL/min	C_{drug} mg/mL	M_{drug} mg	Solvent	M_{MCC} g	$R_{CO2/solution}$ g/mL	D_{MCC} μm
80–150	35–50	0.25–1.5	2.5–15	25–100	3	1–4	16.7–83.3	175–444

Table 2
Details of experimental parameters.

Exp. No.	P bar	T °C	F_{drug} mL/min	C_{drug} mg/mL	M_{drug} mg	Solvent	M_{MCC} g	F_{CO2} g/min	D_{MCC} μm
1	120	40	0.5	5	50	EtOH	2	25	295
2	80	40	0.5	5	50	EtOH	2	25	295
3	150	40	0.5	5	50	EtOH	2	25	295
4	120	35	0.5	5	50	EtOH	2	25	295
5	120	50	0.5	5	50	EtOH	2	25	295
6	120	40	0.3	5	50	EtOH	2	25	295
7	120	40	1	5	50	EtOH	2	25	295
8	120	40	1.5	5	50	EtOH	2	25	295
9	120	40	0.5	2.5	50	EtOH	2	25	295
10	120	40	0.5	10	50	EtOH	2	25	295
11	120	40	0.5	15	50	EtOH	2	25	295
12	120	40	0.5	5	25	EtOH	2	25	295
13	120	40	0.5	5	75	EtOH	2	25	295
14	120	40	0.5	5	100	EtOH	2	25	295
15	120	40	0.5	5	50	MeOH	2	25	295
16	120	40	0.5	5	50	Acetone	2	25	295
17	120	40	0.5	5	50	EtOH	1	25	295
18	120	40	0.5	5	50	EtOH	4	25	295
19	120	40	0.5	5	50	EtOH	2	12.5	295
20	120	40	0.5	5	50	EtOH	2	40	295
21	120	40	0.5	5	50	EtOH	2	25	444
22	120	40	0.5	5	50	EtOH	2	25	175
23[a]	0	50	0.5	5	500	EtOH	20	0	295

[a] Test 23: conventional fluidized bed coating process for comparison; EtOH = ethanol; MeOH = methanol.

Glatt® mini-fluidized bed coater with bottom spray apparatus; 0.5 g talc was added to prevent static. The atomizing nozzle was located at the centre of the lower plenum with a diameter of 0.5 mm. The coating solution was precisely introduced into the nozzle using a syringe pump. The coating operating conditions were close to ambient pressure, 50 °C, compressed air flow rate of 30 m^3/h, atomizing air flow rate of 0.5 m^3/h and coating solution injection rate: 500 μL/min.

2.6. Particle characterization

2.6.1. Quantitative determination of drug loading

The loading of naringin on MCC (mg naringin/g MCC) was measured using a UV detector (UV-2075 plus, Jasco, Japan) by quantitatively dissolving the coated sample in an appropriate solvent, measuring the absorbance of the solution at the specific wavelength (283 nm) and comparing the response with a standard curve (R^2 = 0.9999). The loading of the naringin on MCC was then determined by back calculation.

2.6.2. SEM

Naringin coated MCC and unprocessed naringin samples were deposited onto double sided tape and sputtered with platinum at pressure of 0.5 mbar for 120 s. SEM images were taken using a Philips XL30 ESEM-FEG electron microscope [Philips, Netherlands] fitted with an Oxford Inca 300 EDS system [Oxford Instruments, UK]. The imaging was performed at 5–10 kV and 10 mA.

2.6.3. SPM

A scanning probe microscope (SPM) (NanoWizard II, JPK, Cambridge, UK) was used to acquire the topography of MCC, SASFB process coated and traditional process coated MCC. The SPM measurements were carried out in an ambient environment in intermittent contact mode, using cantilevers (MikroMasch, Germany) with a spring constant of 7 N/m.

2.6.4. XRD analysis

Processed and unprocessed naringin XRD diffraction patterns were collected by an XRD diffractometer (Philips, Xpert-pro, the Netherlands) with a rotating anode and Cu Kαk radiation generated at 30 mA and 40 kV over the 2θ range from 5° to 80°.

2.6.5. FT-IR analysis

Processed naringin and unprocessed naringin were mixed with KBr at 1% naringin/KBr (w/w) separately and pressed to obtain self-made discs which were then characterized by FTIR (IRAFFINITY, Shimadzu Co.) Spectra were collected over 4000–600/cm wavenumbers at a resolution of 4/cm.

2.6.6. In vitro dissolution studies

The tests used simulated gastric fluid (0.1 M hydrochloric acid aqueous solution) as dissolution medium and were carried out in 200 mL of such fluid. The samples evaluated consisted of particles from four different conditions as follows: SAS fluidized bed process naringin coated MCC (designated as SAS-FB), a physical mixture of unprocessed naringin with excipient of 1:1 lactose and MCC (designated as Mixture), conventional fluidized bed preparated naringin coated MCC (designated as FB) and unprocessed naringin (designated as API). The stirring temperature and speed were set at 37 ± 0.5 °C and 35 rpm, respectively. At the sampling time of 1, 3, 5, 10, 20, 30, 45 and 60 min, 3 mL aliquots were taken and replaced by 3 mL dissolution medium. All solutions prepared for analysis were filtered through a 0.22 μm nylon membrane before analysis. The concentration of the naringin was determined by an

ultraviolet spectrophotometer (UNICO 2100, UNICO®, NJ08810, USA). The absorbance of the standard and sample was measured at the maximum absorption wavelength of naringin (283 nm). The amount of naringin in the solution was calculated by a calibration curve ($R^2 = 0.9999$), which was prepared by using standard solutions in the appropriate concentration range. Each point was the average of triplicate tests.

3. Results and discussion

3.1. Operation of the fluidized bed

As noted earlier, the bed used in this work was of very small dimensions (base diameter 6.5 mm) and a truncated cone in shape, compared with that used for studies of fluidization behavior by, for example, Vogt et al. [14] (using cylindrical columns of 21 or 39 mm diameter). The shape was chosen in order to enhance the circulation of the excipient particles, which is usual in fluidized bed coating processes in order to ensure uniform coating and prevent agglomeration. Both the scale and shape of the bed, and its operation within a pressure vessel, prevented accurate measurement of minimum fluidization velocity under operating conditions. It was possible, however, to determine by visual observation the minimum operating velocity necessary for particle circulation, U_C; results are presented in Fig. 3; U_C is here based on the total fluid flow through the bed and is referenced to the cross section at the base. The values are comparable with minimum fluidization velocities measured and calculated for group B particles by Vogt et al. It is observed that the minimum circulation velocity increases with bed mass, which is partially attributed to the shape of the bed.

It is of note here that although all three size cuts of the excipient particles were within the range normally associated with Geldart's "group B" (exhibiting no expansion before bubbling, at ambient conditions) some apparently homogeneous expansion was observed for all sizes as the gas velocity was increased. This is in agreement with the observations of Vogt et al.

The coating experiments were conducted at gas velocities between 1 and $3.8U_C$, with the majority being undertaken at $1.9U_C$ (this relates to the standard condition of 120 bar, 40 °C, 25 g/min CO_2 and 2 g MCC). In all cases, homogeneous expansion had given way to bubbling at this velocity.

3.2. SEM morphology of SAS-fluidized bed coating particles

The morphology of the nanoparticles on the surface of the MCC was evaluated using SEM. Micrographs of a typically coated MCC particles made by test 14 in Table 2 and an uncoated reference MCC particle treated by the SAS fluidized bed process at the same conditions as the coated sample, but without naringin added to the system, are shown in Fig. 4. For comparison, unprocessed API and conventional fluidized bed coated MCC prepared by test 23 (see Table 2) are also shown in Fig. 4.

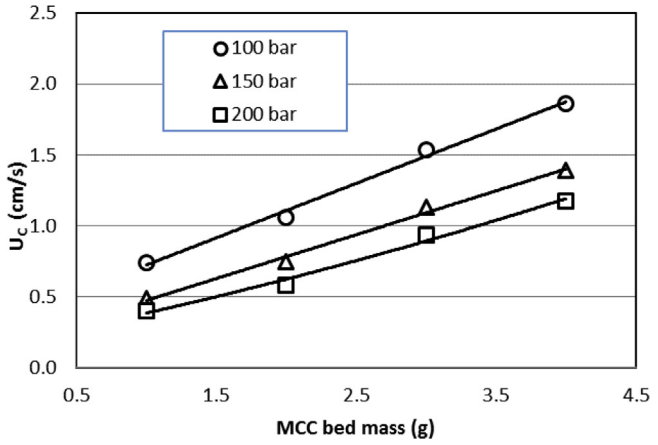

Fig. 3. Minimum circulation velocity, U_c over a range of pressures at 40 °C. Velocity based on base cross-section.

Uncoated MCC (particle size: 295 μm) in Fig. 4(a) exhibits a nearly spherical, smooth surface. The coated MCC in Fig. 4(b)–(d) produced using SASFB show the typical morphology of the naringin particles on the coated surface at different magnifications. High magnification imaging (Fig. 4(e)) shows that the coating consists of particles between 100 and 200 nm, which are reduced from their original size (which had dimensions of $14 \times 10 \times 2$ μm) as shown in Fig. 4(f). The small particle size can be attributed to the way the particles were produced by the SAS process. When the organic solution containing naringin enters the fluidized bed, the solvent is immediately mixed with the sc-CO_2, causing rapid formation of naringin nuclei which contact and adhere on the MCC surface, restricting further growth. Fig. 4(c)–(e) also show that several layers of the 100–200 nm nanoparticles are formed and appear to have platelet-type morphology (Fig. 4(e)). Conversely, in the conventional fluidized bed, when the solution enters the fluidized bed, the solution wets the excipient surface and the solvent is then evaporated by the hot fluidizing air. A continuous layer of naringin without discrete particles is formed over the MCC surface, as shown in Fig. 4(g) and (h).

3.3. SPM of particles on MCC

In addition to SEM, SPM was used to confirm the coating of MCC (295 μm) with naringin nanoparticles (≈100 nm). During SPM measurement, a sharp cantilever with tip radius of ~10 nm was employed to scan the sample surface. MCC samples treated under different processes were analysed. The results of SPM are shown in Fig. 5, in which Fig. 5(a) shows the surface of the uncoated MCC spheres. It was found that the MCC surface is composed of agglomerates of the cellulose matrix of around 7 μm. Fig. 5(b) shows the Naringin-covered morphology of the MCC surface prepared by the conventional fluidized bed approach of test 23 in Table 2, which results in flake-like objects of micron size; this is consistent with the results shown in Fig. 4(g) and (h). Fig. 5(c) shows Naringin-coated MCC prepared by the SAS fluidized bed process of test 7 in Table 2. It confirms that the MCC surface was covered with spherical structures with a diameter of approximately 100 nm.

3.4. Characterization of nanosized naringin

Samples of processed and unprocessed naringin underwent FT-IR and XRD analyses to ascertain any change to chemical structure during processing. The FT-IR results are shown in Fig. 6, where the blue line labelled "Naringin SAS" is SAS fluidized bed processed material, while the red line labelled "Naringin API" is unprocessed (as-received) naringin. The scan results show no significant difference. The results of the XRD are shown in Fig. 7 with the same notation for the samples as in Fig. 6. It can be seen that processed naringin lost all characteristic peaks, changing from crystalline to amorphous during processing as the precipitation process is too fast for the crystal structure to order itself.

3.5. Dissolution profiles of processed and unprocessed naringin

Fig. 8 shows the release rate curves of naringin from SAS fluidized bed particles (SAS-FB) made by test 10 in Table 2, API as-received (API), a physical mixture of the excipient (1:1 lactose and MCC) and API (i.e. uncoated) at the same naringin content as

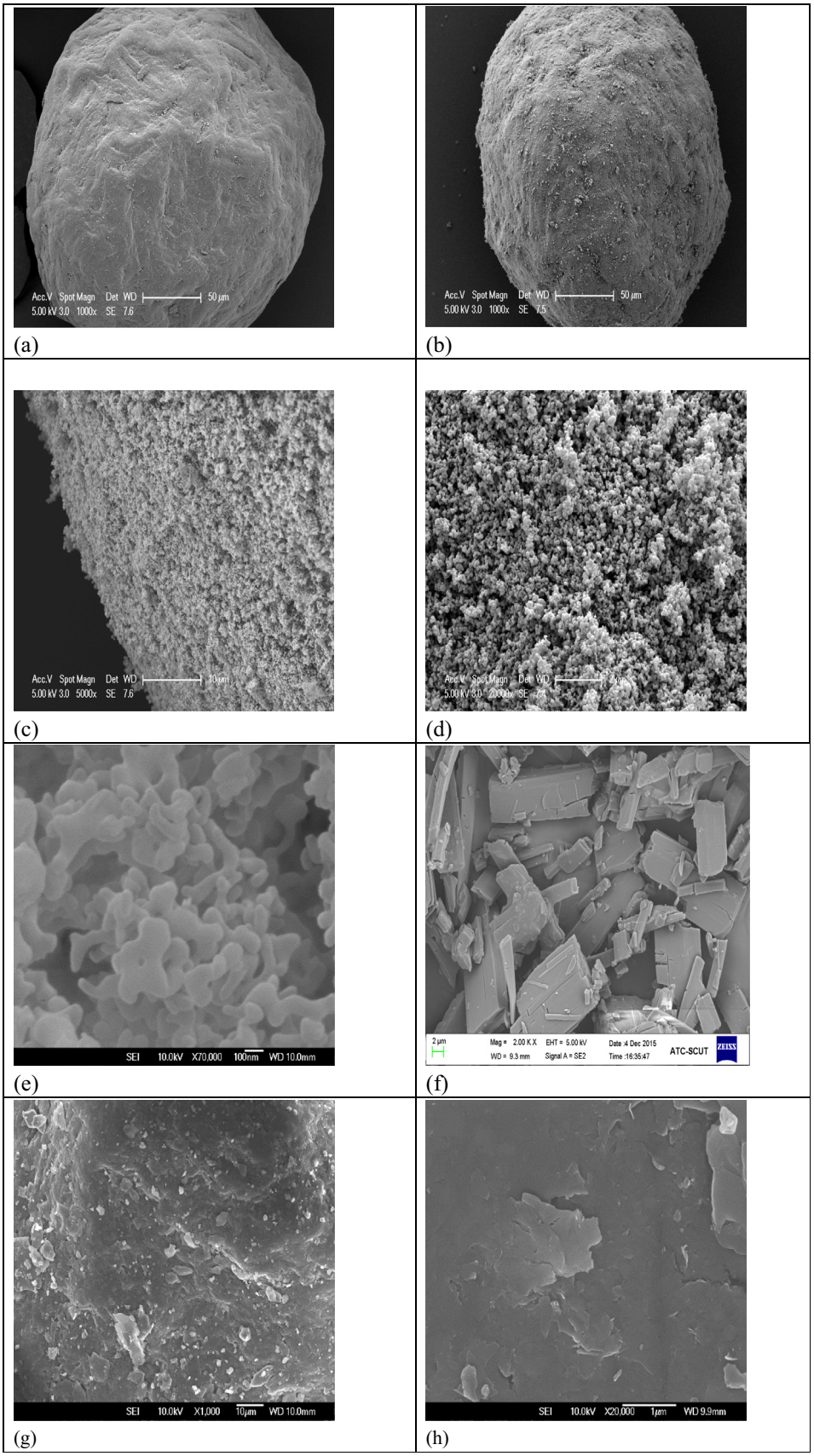

Fig. 4. SEM images of uncoated MCC, naringin coated MCC, and original naringin. Assays: (a): uncoated reference MCC (295 μm, processed with ethanol). (b): naringin coated MCC (made by test 14 in Table 2; 5 mg/mL) at magnification 1000×; (c): at 5000×; (d): at 20,000× and (e): at 70,000×. (f): untreated naringin API. (g): conventional fluidized coating MCC (made by test 23 in Table 2) at magnification 1000× and (h): at 20,000×.

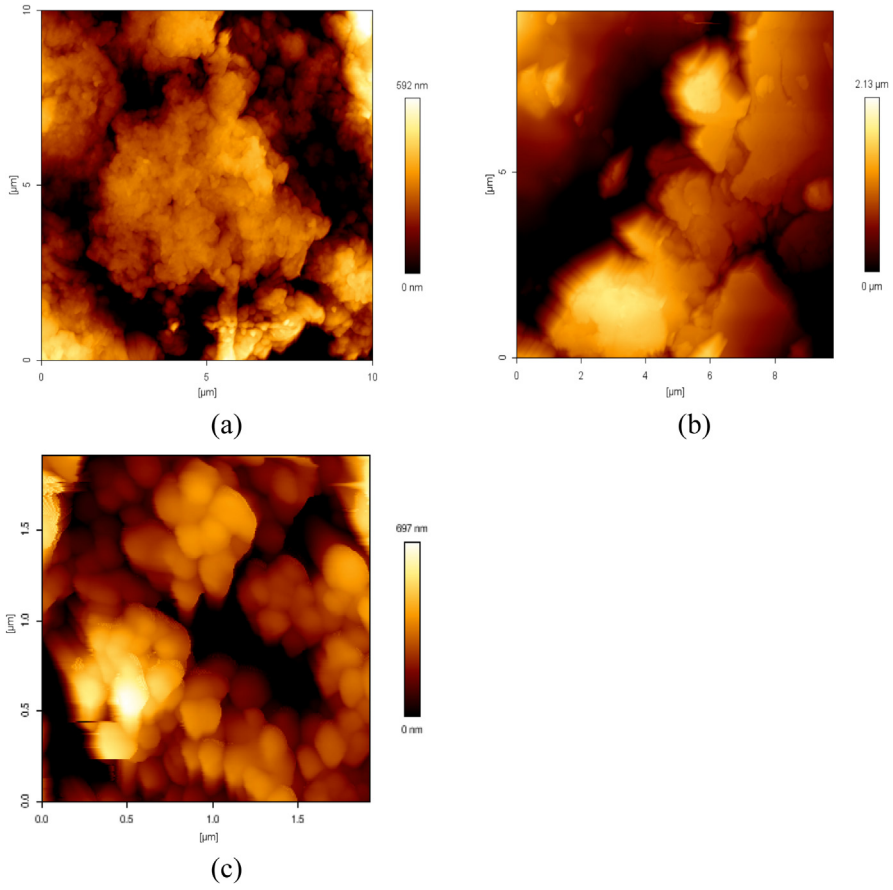

Fig. 5. Coating results by SPM. Assays: (a) Uncoated MCC (295 µm) surface. (b) Surface of naringin coated MCC obtained from conventional fluidized bed coating, test 23 in Table 2; 5 mg/mL. (c) Surface of naringin coated MCC obtained from SASFBC coating test 7 in Table 2; 5 mg/mL.

the loading of SAS fluidized bed particles (Mixture) and conventional fluidized bed particles (FB) made by test 23 in Table 2. Fig. 8(a) and (b) show that the release rate of naringin coated on MCC by the SAS fluidized bed process is faster than all three other approaches and has the highest release ratio. The nanoparticles released 90% of the API in the first minute and become stabilized at c. 100% in 3 min, while the as-received API and the API + excipient mixture give release less than 45% in the first minute and had not completely stabilized at 60 min. The conventional fluidized bed particles (FB) give 80% release in the first minute and become stabilized at c. 90% in 3 min. The results show that the naringin nanoparticles on the MCC produced by the SAS fluidized bed process lead to almost immediate naringin release.

3.6. The effect of SAS fluidized bed process parameters on naringin dissolution profiles

The particle size obtained by the SAS process is affected by the process parameters. During a SAS fluidized bed process, the MCC excipient in the fluidized bed captures a substantial proportion of the nuclei, so restricting their further growth. In tests without the fluidized bed the SAS process alone gave agglomerated particles that were "fluffy" in nature, with a very low bulk density and sizes of approximately 1–2 mm wide and 5 mm in length; this demonstrates the clear advantage of the SAS fluidized bed process at restricting particle agglomeration.

The enhanced release rate of naringin is a significant outcome of the SAS fluidized bed process due to the particle size, morphology, loading and degree of aggregation of API on the MCC excipient. No direct comparison of the SAS fluidized bed process parameters on drug release can be made with the literature as this is the first time this process has been reported; however the results in Fig. 9 can be used for future work and process design. It can be seen that there is a high immediate release rate for all samples over the range of process conditions. It is evident, however, that the release profiles correlate with the process parameters. Fig. 9a shows the effects of process pressure on drug release. It is clear that there is an optimum process pressure; with all other parameters constant, as the pressure increases (tests 1, 2 and 3 in Table 2), the final release of naringin increases to its maximum at 120 bar then decreases. Fig. 9b shows release rates of samples made by tests 1, 4 and 5 in Table 2 operated at three temperatures and the data show that a process temperature between 40 and 50 °C results in a product with faster release than that produced at 35 °C. Fig. 9c shows that the naringin solution flow rate within the test range (tests 1, 6, 7 and 8) has almost no effect on the release rate.

Fig. 9d shows that for the range of drug concentrations (tests 1, 9, 10 and 11) release ratios >95% were achieved with 10 mg/ml giving a 5% higher value. The drug concentration generally has a small effect on the release rate. It was observed that a deeper fluffier coating layer resulted when lower concentrations of naringin solution were used. Due to the porous structure, water molecules can be easily transported through the shell, resulting in an accelerated dissolution. The dissolution rate therefore increases as the naringin concentration increases, from 2.5 to 10 mg/mL. When the naringin concentration was increased to 15 mg/mL, closer packing and agglomeration of particles is observed; this can be seen by comparing the images in Fig. 10. Due to the agglomeration, and the closer

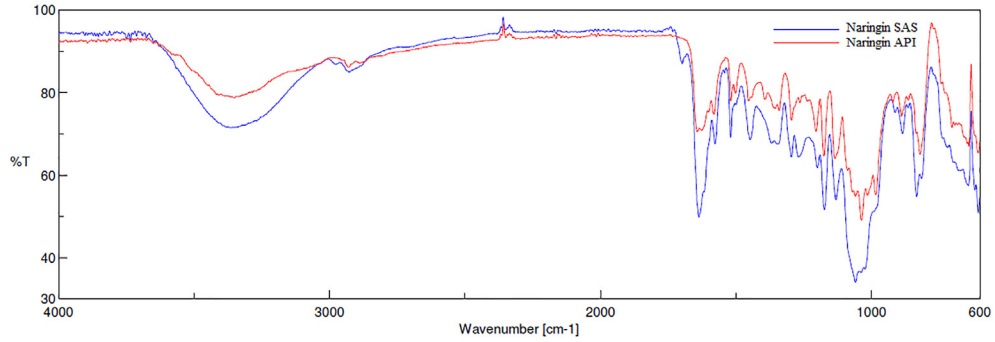

Fig. 6. FT-IR spectra of naringin API (red) and SASFBC processed naringin (blue). (For interpretation of the references to colour in this figure legend, the reader is referred to the web version of this article.)

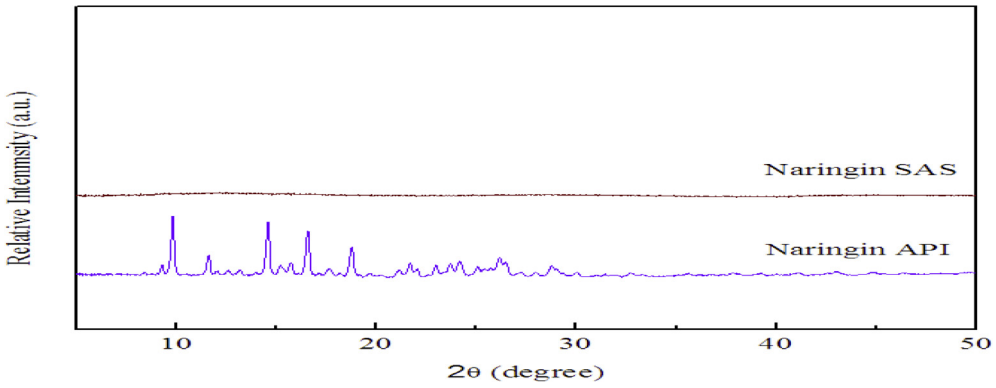

Fig. 7. XRD patterns of naringin API (below) and SASFBC processed naringin (top).

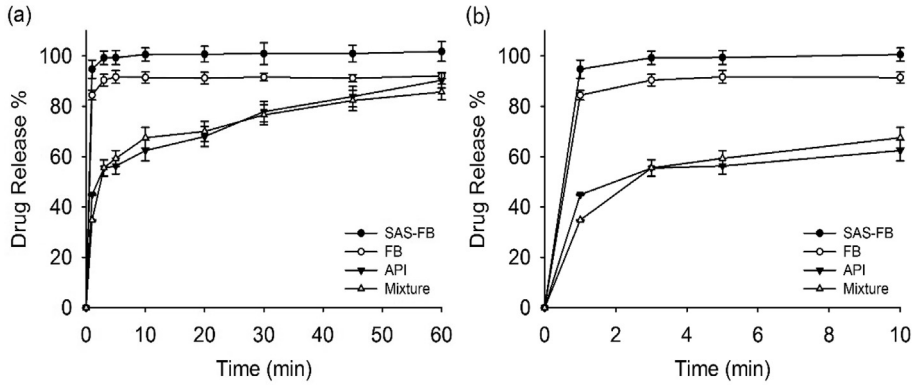

Fig. 8. The effect of different methods on dissolution rate. (a) SAS fluidized bed particles (SAS-FB), physical mixture particles (Mixture), API particles (API) and conventional fluidized coating particles (FB) release curves in 60 min; (b) SAS fluidized bed particles, physical mixture particles, API particles and conventional fluidized coating particles release 0–10 min release curves;

proximity of particles it becomes more difficult to transport water and the overall dissolution rate decreases. Lower relative concentrations are therefore beneficial to API release.

Fig. 9e shows that when the total drug used is between 2.5 and 5 wt% of the excipient mass (tests 1, 12 and 13), the coating shows better properties than when a lower feed 1.25 wt% of excipient mass (test 14) is used.

The API solubility depends on the particular organic solvent. The solubility of naringin has been given by Zhang et al. [21] as 24.4 mg/mL (20 °C) and 28.6 mg/mL (25 °C) in methanol. Furthermore, Naringin can completely dissolve in ethanol, methanol and acetone at the maximum concentration of 15 mg/mL used in the experiments. Higher concentrations of naringin, between 20 and 30 mg/mL, were observed to dissolve. The polarisation differences between ethanol, methanol and acetone lead to different solubilities in supercritical carbon dioxide, and will influence the SAS process and the subsequent dissolution and release rates. Fig. 9f (tests 1, 15 and 16) shows indirectly the effect of solvent choice (and indirectly the solubility) on the coating results. Ethanol, acetone and methanol are all suitable for the coating process with all three solvents producing similar particles; however as seen in Fig. 9f acetone gave the highest release rate.

The geometric shape of fluidized bed was fixed, and therefore, the height of fluidized bed is dependent on the mass of MCC used. Fig. 9g shows that MCC masses of 1–4 g (tests 1, 17 and 18) all gave acceptable coating results (as indicated by the release rate)

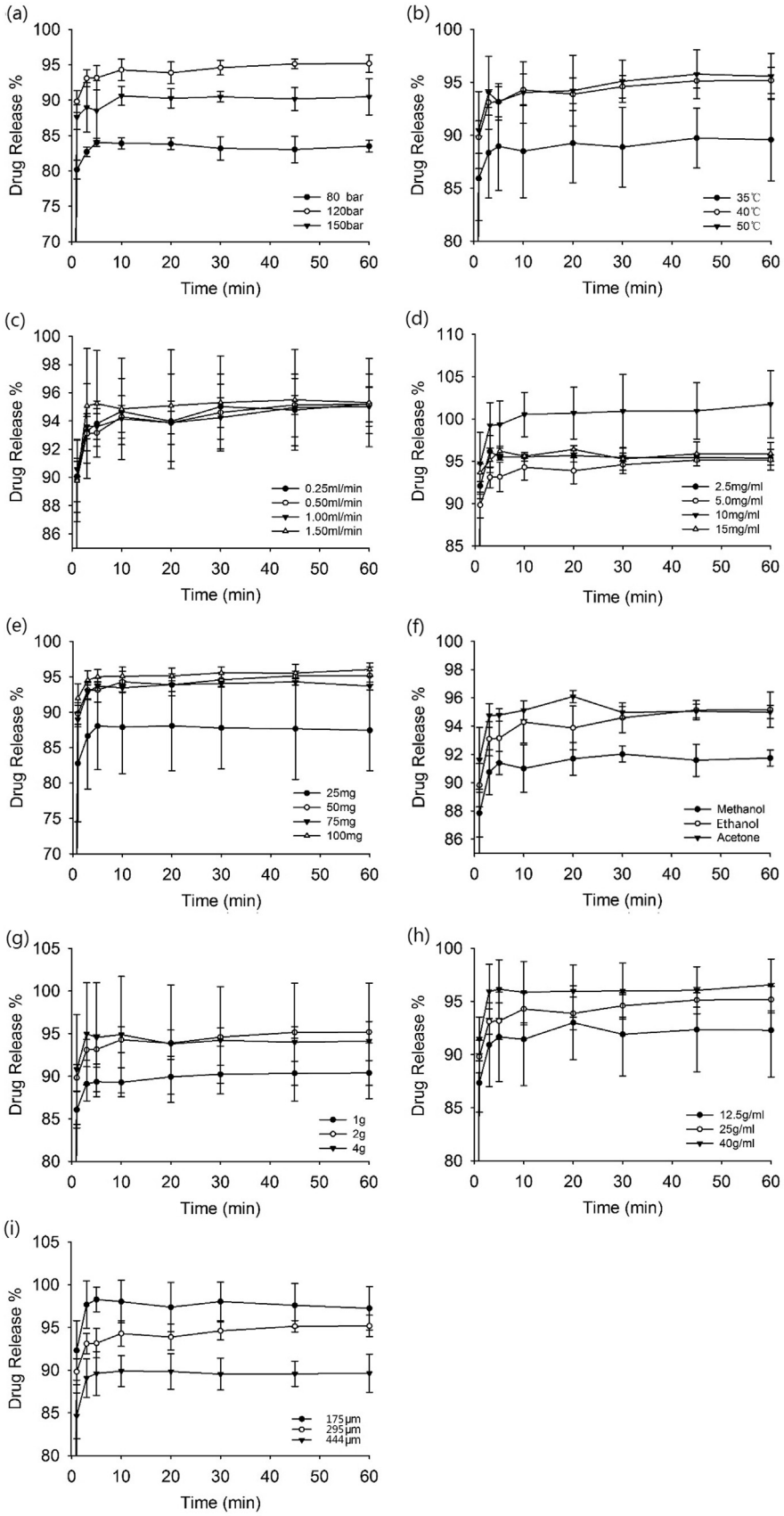

Fig. 9. The effect of different process parameter on release rate. Read in conjunction with Table 2. (a) Effect of coating pressure; samples prepared from tests 1, 2 and 3. (b) Effect of coating temperature; samples prepared from tests 1, 4 and 5. (c) Effect of drug solution flow rate; samples prepared from tests 1, 6, 7 and 8. (d) Effect of drug concentration; samples prepared from tests 1, 9, 10 and 11. (e) Effect of drug mass; samples prepared from tests 1, 12, 13 and 14. (f) Effect of solvents; samples prepared from tests 1, 15 and 16. (g) Effect of MCC mass in fluidized bed; samples prepared from tests 1, 17 and 18. (h) Effect of CO_2 flow rate; samples prepared from tests 1, 19 and 20. (i) Effect of MCC diameter samples prepared from tests 1, 21 and 22.

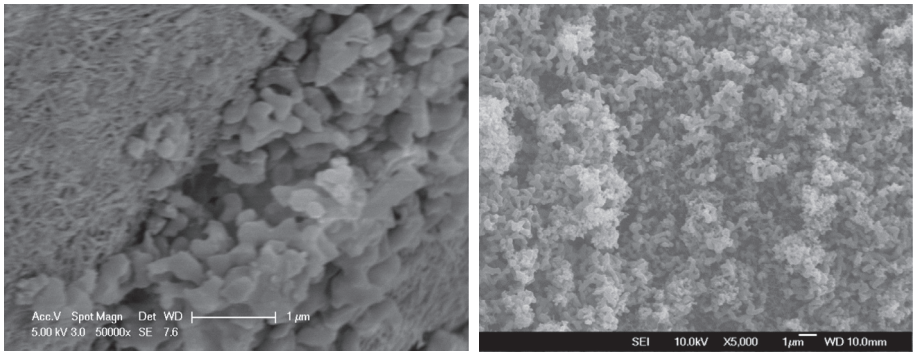

Fig. 10. Micrographs of naringin particles on the surface of MCC at 15 mg/ml (left) and 5 mg/mL (right).

Table 3
Experimental parameters and coating results.

Exp No.	P bar	T °C	Drug solution flow mL/min	C_{drug} mg/mL	Drug total mass fed mg	Solvent	MCC mass g	CO_2 flow rate g/min	D_{MCC} μm	Drug content w/w%	Coating efficiency w/w%
1	120	40	0.5	5	50	EtOH	2	25	295	2.4	96.9
2	80	40	0.5	5	50	EtOH	2	25	295	2.3	90.0
3	150	40	0.5	5	50	EtOH	2	25	295	2.0	81.4
4	120	35	0.5	5	50	EtOH	2	25	295	2.1	85.1
5	120	50	0.5	5	50	EtOH	2	25	295	2.4	96.5
6	120	40	0.3	5	50	EtOH	2	25	295	1.9	75.3
7	120	40	1	5	50	EtOH	2	25	295	2.5	99.2
8	120	40	1.5	5	50	EtOH	2	25	295	2.1	85.5
9	120	40	0.5	2.5	50	EtOH	2	25	295	2.5	99.8
10	120	40	0.5	10	50	EtOH	2	25	295	1.6	62.6
11	120	40	0.5	15	50	EtOH	2	25	295	1.7	66.5
12	120	40	0.5	5	25	EtOH	2	25	295	1.1	89.1
13	120	40	0.5	5	75	EtOH	2	25	295	2.9	77.4
14	120	40	0.5	5	100	EtOH	2	25	295	4.1	81.5
15	120	40	0.5	5	50	MeOH	2	25	295	2.0	77.9
16	120	40	0.5	5	50	Acetone	2	25	295	2.1	82.2
17	120	40	0.5	5	50	EtOH	1	25	295	4.1	82.3
18	120	40	0.5	5	50	EtOH	4	25	295	1.2	91.9
19	120	40	0.5	5	50	EtOH	2	12.5	295	1.1	44.6
20	120	40	0.5	5	50	EtOH	2	40	295	2.0	79.4
21	120	40	0.5	5	50	EtOH	2	25	444	2.2	88.1
22	120	40	0.5	5	50	EtOH	2	25	175	1.1	44.4
23[a]	0	50	0.5	5	500	EtOH	20	0	295	1.6	65.8

[a] 23: Conventional fluidized coating.

although the 1 g bed produced a product with a slightly slower release and 5% lower release ratio than the 2 and 4 g beds.

The gas flow rate is a key parameter in fluidizing the bed and hence the efficacy of the process. Its effect on the product properties resulting in active release (tests 1, 19 and 20) are shown in Fig. 9h. A CO_2 flow above 12.5 g/min (1.1 $U_{C)}$ leads to a product with an acceptable release rate and release ratio as the gas flow rate is sufficient to keep the bed fluidized and circulating the MCC. In this work the higher CO_2 flow rate gave better release rates. The release rates of samples from tests 1, 21 and 22 using three different sizes of MCC are shown in Fig. 9i. The effect of MCC diameter in the coating process on the product release rate shows a tendency for the smaller size of MCC particles to have a faster release rate. The release rates of large diameter MCC particles is relatively low, probably due to its lower specific surface area.

3.7. The effect on drug content and coating ratio

Although the product release rate is the ultimate indicator for judging the success of the process in this work, the drug content (ratio of drug mass to MCC mass) and coating efficiency (ratio of drug coated on MCC to total feed) are other key indicators. The coating efficiency was influenced by the MCC particle size with the smaller 175 μm particle leading to low efficiencies as a result of the smaller surface area available per particle. Poorly adhered naringin would have been carried out in the CO_2 stream during the CO_2 "wash" step at the end of the process as evidenced by the collection of particles on the filter downstream of the bed.

Table 3 lists the drug content and coating efficiency of all tests. It is convenient to see the effect of operational parameters on coating results and this table complements the data shown in Fig. 9.

Table 3 shows the drug content and coating efficiency of the SAS-fluidized bed process to coat naringin on MCC. The drug loadings are between 1.1 and 4.1 w/w% and the coating efficiency can reach 99.8% (test 9) when all the parameters are optimized. Over the entire operational range, half the tests gave coating efficiencies of more than 85%. In comparison, the conventional fluidized bed coating method gave loadings of 1.6% and a coating efficiency of 65.8% at the conditions studied, which are less than the SAS-fluidized bed process.

4. Conclusion

High release rates of a drug compound with low water solubility can be obtained using the supercritical anti-solvent fluidized

bed process developed in this work. The new process gave better results than a conventional fluidized bed coating process using the same starting materials. The process results in a product consisting of excipient carrier particles coated in nano-sized drug particles. SEM study showed that the nanoparticles of naringin have a typical spherical morphology with particle sizes between 100 and 200 nm. SPM also confirmed that the surface was covered with spherical structures with a diameter of approximately 100 nm. XRD showed that naringin changes from crystalline to amorphous during processing.

The work demonstrates the advantages of the combined fluidized bed and supercritical anti-solvent process and offers a new alternative approach to production of a product form with favorable drug release profile. The dissolution tests demonstrated that there are significant differences between the products of SAS-fluidized bed process and coated particles produced by conventional routes. The results showed that the naringin nanoparticle coatings result in products which show immediate release, with a cumulative dissolution of 90% in the first minute and 100% in 3 min. Thus, the SAS-fluidized bed process substantially increased both the cumulative dissolution and dissolution rates of naringin.

Since the drug content of Naringin-coated MCC prepared by the SAS-fluidized bed is around 2.5 wt%, it could be directly administered orally, if desired. Downstream processes such as granulation and tableting, which carry risks of causing nanoparticle agglomeration or further changes in the crystal form might therefore be unnecessary.

Datasets

Data underlying this study can be accessed through the Cranfield University repository at 10.17862/cranfield.rd.4480199.

Acknowledgement

The authors acknowledge the financial support from EPSRC (EP/F037228/1), the School of Chemical Engineering, University of Birmingham, and the School of Chinese Materia Medica, Guangzhou University of Chinese Medicine.

The scanning probe microscope used in this research was obtained, through Birmingham Science City: Innovative Uses for Advanced Materials in the Modern World (West Midlands Centre for Advanced Materials Project 2), with support from Advantage West Midlands (AWM) and part funded by the European Regional Development Fund (ERDF). Prof. Shixia Guan of the Guangzhou University of Chinese Medicine, Dr. Jason Zhang, Dr. Shangfeng Du and are acknowledged for helpful discussions and insightful suggestions. We also acknowledge earlier discussions with Dr Rachel Bridson. The authors also would like to thank Dr. Ji Zou, Miss Jing Wu and Mr. Evangelos Liamas for providing technical guidance with SEM and SPM.

References

[1] A.H. Junghanns, R.H. Müller, Nanocrystal technology, drug delivery and clinical applications, Int. J. Nanomed. 3 (2008) 295–309.
[2] F. Kesisoglou, S. Panmai, Y. Wu, Nanosizing Oral formulation development and biopharmaceutical evaluation, Adv. Drug Deliv. Rev. 59 (2007) 631–644.
[3] P.G. Debenedetti, J.W. Tom, S.-D. Yeo, G.-B. Lim, Application of supercritical fluids for the production of sustained delivery devices, J. Control. Release 24 (1993) 27–44.
[4] K. Westesen, H. Bunjes, M.H.J. Koch, Physicochemical characterization of lipid nanoparticles and evaluation of their drug loading capacity and sustained release potential, J. Control. Release 48 (1997) 223–236.
[5] J. Jung, M. Perrut, Particle design using supercritical fluids: literature and patent survey, J. Supercrit. Fluids 20 (2001) 179–219.
[6] Y. Hakuta, H. Hayashi, K. Arai, Fine particle formation using supercritical fluids, Curr. Opin. Solid State Mater. Sci. 7 (2003) 341–351.
[7] T. Lu, S. Blackburn, C. Dickinson, M.J. Rosseinsky, G. Hutchings, S. Axon, G.A. Leeke, Production of titania nanoparticles by a green process route, Powder Technol. 188 (2009) 264–271.
[8] A.A. Thorat, S.V. Dalvi, Liquid antisolvent precipitation and stabilization of nanoparticles of poorly water soluble drugs in aqueous suspensions: recent developments and future perspective, Chem. Eng. J. 181–182 (2012) 1–34.
[9] N. Mezzomo, S.R.R. Comim, C.E.M. Campos, S.R.S. Ferreira, Nanosizing of sodium ibuprofen by SAS method, Powder Technol. 270 (2015) 378–386.
[10] Y. Zu, Q. Zhang, X. Zhao, D. Wang, W. Li, X. Sui, Y. Zhang, S. Jiang, Q. Wang, C. Gu, Preparation and characterization of vitexin powder micronized by a supercritical antisolvent (SAS) process, Powder Technol. 228 (2012) 47–55.
[11] E. Reverchon, G.D. Porta, Production of antibiotic micro- and nano-particles by supercritical antisolvent precipitation, Powder Technol. 106 (1999) 23–29.
[12] G.A. Leeke, T. Lu, R.H. Bridson, J.P.K. Seville, Application of nano-particle coatings to carrier particles using an integrated fluidized bed supercritical fluid precipitation process, J. Supercritical Fluids 91 (2014) 7–14.
[13] R. Schreiber, C. Vogt, J. Werther, G. Brunner, Fluidized bed coating at supercritical fluid conditions, J. Supercrit. Fluids 24 (2002) 137–151.
[14] C. Vogt, R. Schreiber, G. Brunner, J. Werther, Fluid dynamics of the supercritical fluidized bed, Powder Technol. 158 (2005) 102–114.
[15] R. Schreiber, B. Reinke, C. Vogt, J. Werther, G. Brunner, High-pressure fluidized bed coating utilizing supercritical carbon dioxide, Power Technol. 138 (2003) 31–38.
[16] K. Rosenkranz, S. Rodriguez-Rojo, M.M. Kasper, J. Werther, G. Brunner, Zweistufige Mikroverkapselung von Rinderserumalbumin auf Tragerpartokeln in der Hochdruckwirbelschicht, Chem. Ing. Teck. 79 (2007) 313–319.
[17] V. Martin, R. Romero-Diez, S. Rodriguez-Rojo, M. Jose Coero, Titanium dioxide nanoparticle coating in fluidized bed via supercritical anti-solvent process (SAS), Chem. Eng. J. 279 (2015) 425–432.
[18] Y.-C. Nie, H. Wu, P.-B. Li, Y.-L. Luo, K. Long, L.-M. Xie, J.-G. Shen, W.-W. Su, Anti-inflammatory effects of naringin in chronic pulmonary neutrophilic inflammation in cigarette smoke-exposed rats, J. Med. Food 15 (2012) 894–900.
[19] E.J. Choi, J.I. Lee, G.H. Kim, Effects of 4′,7-dimethoxyflavanone on cell cycle arrest and apoptosis in human breast cancer MCF-7 cells, Arch. Pharm. Res. 34 (2011) 2125–2130.
[20] G.N. Pulley, Solubility of Naringin in Water, U.S. Dept. of Agriculture, Bureau of Agricultural and Industrial Chemistry, USA, 1945.
[21] L.Q. Zhang, L. Song, P.P. Zhang, T.T. Liu, L. Zhou, G.D. Yang, R. Lin, J.Y. Zhang, Solublilities of Naringin and Naringenin in different solvents and dissociation constants of Naringin, J. Chem. Eng. Data 60 (2015) 932–940.

Supercritical fluid coating of API on excipient enhances drug release

Li, Qingguo

2016-12-18

Li Q, Huang D, Lu T, Seville JPK, Xing L, Leeke GA, Supercritical fluid coating of API on excipient enhances drug release. Chemical Engineering Journal, Volume 313, 1 April 2017, pp. 317-327
http://dx.doi.org/10.1016/j.cej.2016.12.066